Dynamic behaviour of cavitation bubble close to a flexible wall

Miloš Müller[1*], *Jan* Hujer[1], and *Petra* Dančová[1]

[1]Department of power engineering equipment, Technical University of Liberec, Studentská 1402/2, 461 17 Liberec 1, Czech Republic

Abstract. The dynamic behaviour of cavitation bubble close to a flexible boundary is investigated experimentally. The cavitation bubble is produced as a consequence of an optical breakdown generated by the focus of 532 nm Nd-Yag laser beam. A gold mirror is used to focus the expanded laser beam into a spherically shaped plasma. A PVDF film sensor is used for the measurement of the interaction magnitude between the bubble and the flexible boundary. As the flexible boundary directly the PVFD film sensor is used. The sensor is flexibly mounted within a specially designed movable frame which enables to modify the elastic properties of the system. The bubble dynamics and the flexible wall movement are recorded by high-speed CCD camera and correlated with the acoustic signal obtained by the PVDF film. Different bubble collapse patters for different bubble wall distances and the corresponding acoustic signals are presented.

1 Introduction

In the last decades, the laser induced breakdown LIB [1] and its interaction with the biological tissue have been intensively studied [2], [3], [4], [5], [6]. This interest was motivated by the importance of the effects accompanying the LIB, the shock waves and cavitation bubbles. The determination of the type of interaction between the cavitation bubble and the flexible wall during the bubble collapse is important in order to estimate the damage potential of the collapsing bubble and also the range of the wall deformation.

For the solid wall it is considered that the bubble wall interaction is realised by three main effects [7]. The first effect is a fast liquid microjet formed during the bubble rebound after the collapse. In the case of solid wall this jet is directed towards the wall. This effect is produced by bubbles at medium distance from the wall. The second effect is so called splashing, which is generated by bubbles in direct contact with the solid wall. The shock wave [8], [7] is the last effect responsible for the cavitation erosion. The shock waves can be generated by the bubbles collapsing in the far field but also by bubbles collapsing directly on the wall. In the case of laser induced bubble, the shock wave is usually produced during the bubble initiation [9], [1] as a consequence of the rapid plasma expansion. When the bubble collapses close to a solid boundary, the bubble attraction to the solid wall can also be observed. This attraction is caused by so called "Bjerkens force" [7], [8].

In general, the cavitation bubble can collapse in a free field of liquid or close to a boundary. The magnitude of the bubble impact depends on several parameters, which include the bubble wall distance, the maximum bubble radius and the wall material.

The distance of the bubble inception (LIB) from the boundary s is usually normalized by maximum bubble radius R_{max} in form

$$\gamma = s/R_{max}. \quad (1)$$

Dynamics of a spark generated cavitation bubble close to an elastic boundary was investigated e.g. by Gibson [10], [11]. The author investigated the bubble behaviour close to rigid boundaries with rubber coatings. An important result from their measurements was that for some range of the wall properties no bubble jet was generated during the bubble collapse and the bubble formed an hourglass shape. A cavitation bubble generated by laser near gelatine surface was studied in [12]. The authors observed that the cavitation bubbles inclined not to produce liquid jets and tended to migrate from the surface.

Shima showed in [13] that for some combinations of wall properties and the bubble wall distances no bubble migration occurs. The most comprehensive study of the dynamics of the laser induced cavitation bubble collapsing close to an elastic boundary is given in [14] by Brujan. The author uses polyacrylamide as the wall material. He studied the bubble collapse for large range of γ and identified the ranges where the bubble jet is directed towards the boundary and where the jet is directed away from the boundary. He also measured the jet highest velocities.

2 Experimental setups

The basic setup for the measurement of the interaction between the cavitation bubble and the flexible wall is given in Figure 1. The cavitation bubbles are generated by Nd-Yag laser at wavelength 532 nm focused into the

* Corresponding author: milos.muller@tul.cz

bath. To minimize the spherical abbreviation of the bubble the optical setup with gold spherical mirror was used [15]. The laser beam of diameter 5 mm is firstly expanded trough a Galilean beam expander (4x) and focused trough a gold mirror.

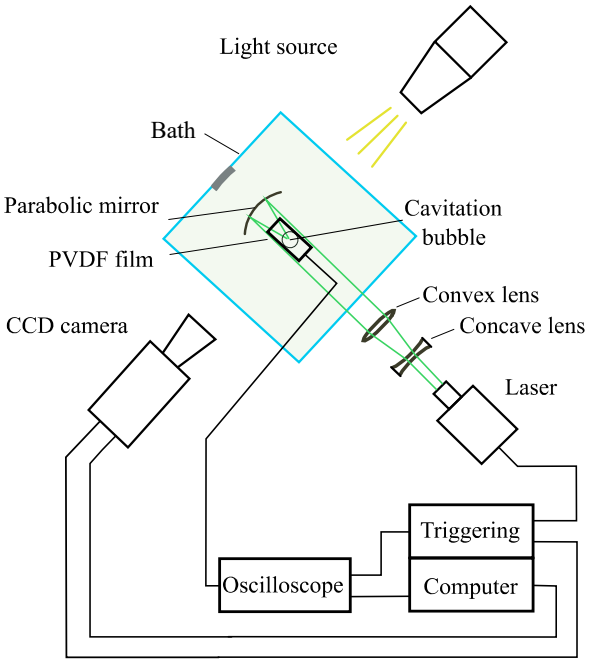

Fig. 1. Experimental setup used in the investigation of the cavitation bubble collapse.

Due to the arrangement of the experiment the LIB is generated out of optical axis to ensure no crossing between the expanded beam and the flexible wall. The cavitation bubble dynamics was investigated by synchronized acoustic and optical measurements.

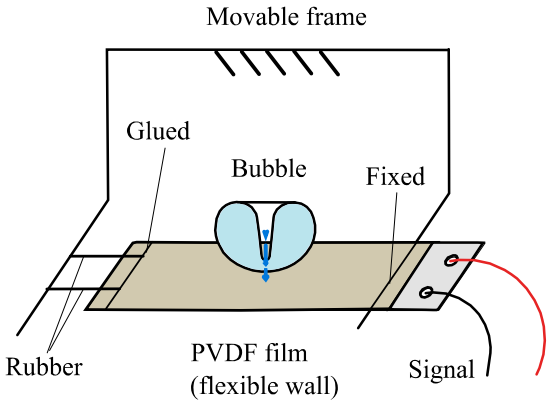

Fig. 2. Flexible wall arrangement.

The optical measurement was based on the high-speed photography using ultra-fast CCD cameras. The bubble collapse illumination was provided by the high-power flash lamp in continuous mode. The lamp was used with the collimating lens to provide the parallel illumination for visualization of the bubble surface. The acoustic measurement was realized with the high sensible piezoelectric polyvinylidene fluoride (PVDF) polymer transducer. The PVDF film was mounted on a movable frame submerged into the water bath and directly used also as the flexible wall. The bath walls were perpendicular to the optical axes. The placement of the PVDF film on the movable frame is shown in Figure 2. The film is mounted between two parallel supports. On one side of the support the film is glued directly on the supporting beam. To the second side of the support the film is connected by two rubber straps, which defines the wall support. To avoid the film deformation between the two rubber straps a wood beam is glued on the film. The film surface was covered with very thin black paint to protect the camera from the beam radiation during the wall deformation. The electrical contacts of the PVDF film are protected by a tape. The elastic modulus of the flexible wall was estimated based on a tensile test to 0.2 MPa.

The sampling frequency for the acoustic measurements was 60 MHz and for the optical measurement 170 kHz. The PVDF film was used to measure the local short time exposure caused by the direct interaction of the PVDF film (flexible wall) and also to measure the long-time tensile load. The PVDF film is not calibrated so only the load character can be identified from the voltage signal. Optical measurements are synchronized by Dynamic Studio (Dantec) software. The acoustic signals are recorded by high-speed oscilloscopic card. NI LabVIEW Signal Express software is used for the acoustic data acquisition and processing.

3 Results

The experimental results are represented in the form of the figures of the time evaluation of the bubble radius and in the form of the PVDF film signals. The individual figure collections correspond to a single value of the relative bubble wall distance γ. Due to the bubble deformation close to the boundary the vertical and horizontal bubble radii were evaluated.

The bubble shape is deformed in the dependence on the distance between the initial position of the bubble centre and the initial wall position.

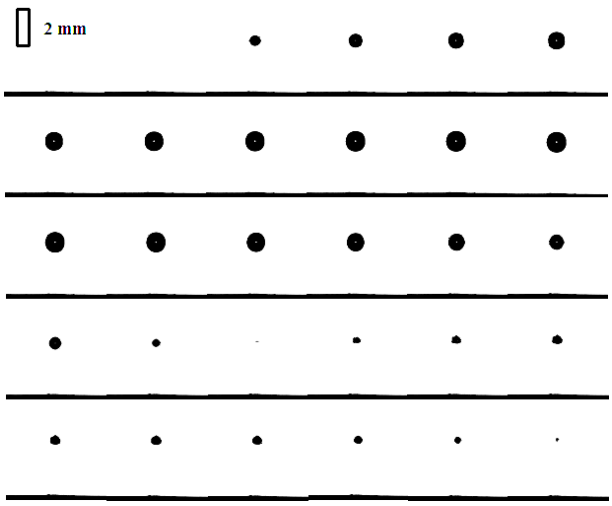

Fig. 3. Bubble dynamics for γ = 4.6. Time between the individual frames is 5.9 µs.

For the bubble wall distance γ = 4.6 (Figure 3) the bubble shape is not influenced by the wall presence. This is also evident in Figure 8 as the vertical and horizontal bubble radii are almost identical. For the bubble wall distance γ = 1.6 (Figure 4) the wall deformation and the bubble deformation are evident. However, the bubble jet in comparison to the rigid wall case is generated towards from the flexible wall.

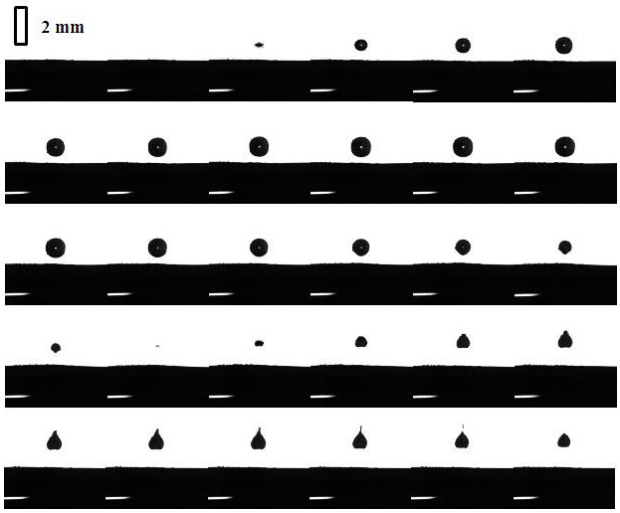

Fig. 4. Bubble dynamics for γ = 1.6. Time between the individual frames is 5.9 µs.

For the bubble wall distance γ = 1.1 (Figure 5) the wall deformation and the bubble deformation in vertical direction are visible. The bubble jet is generated towards the wall but the bubble migrates towards from the wall after the rebound It can be also seen that the bubble is spitted during the jet formation.

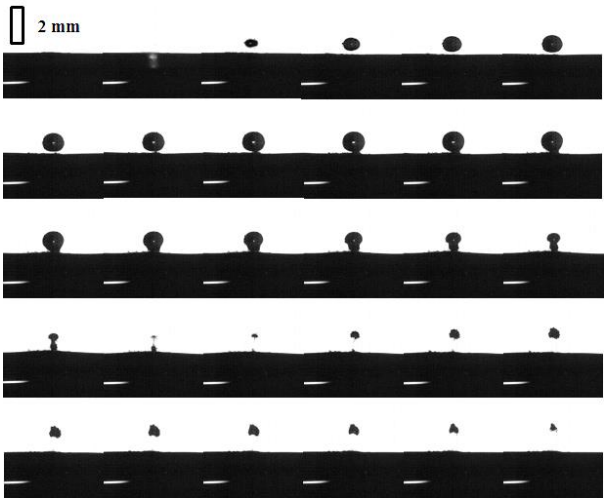

Fig. 5. Bubble dynamics for γ = 1.1. Time between the individual frames is 5.9 µs.

For the bubble wall distance γ = 0.9 (Figure 5) the bubble is in direct touch with the flexible wall. The vertical and horizontal bubble radii are significantly different. Due to the needle bubble shape after the rebound the vertical and horizontal radii are not evaluated in Figure 6.

The first and second bubble expansion and first and second bubble collapse are illustrated in Figure 6. It can be seen that the bubble shape is influenced by the wall presence mainly after the first collapse (the first bubble rebound). During the growth phase after the plasma expansion the bubble is rather spherical. This corresponds to the rigid wall case, where the bubble shape is deformed also during the first rebound.

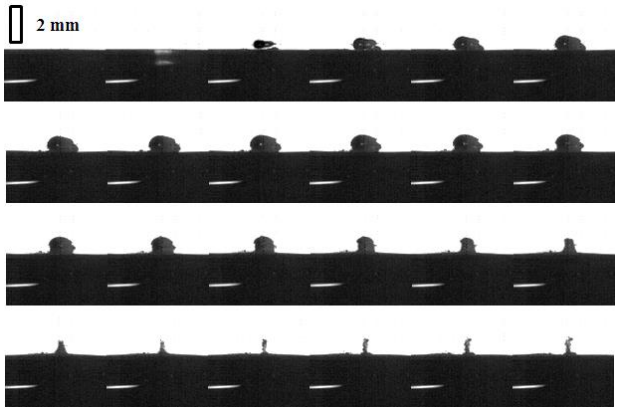

Fig. 6. Bubble dynamics for γ = 0.9. Time between the individual frames is 5.9 µs.

Figure 8 illustrates the voltage signals measured on the PVDF film sensor (flexible wall). The signal can be correlated with the horizontal and vertical bubble radii presented in Figure 7.

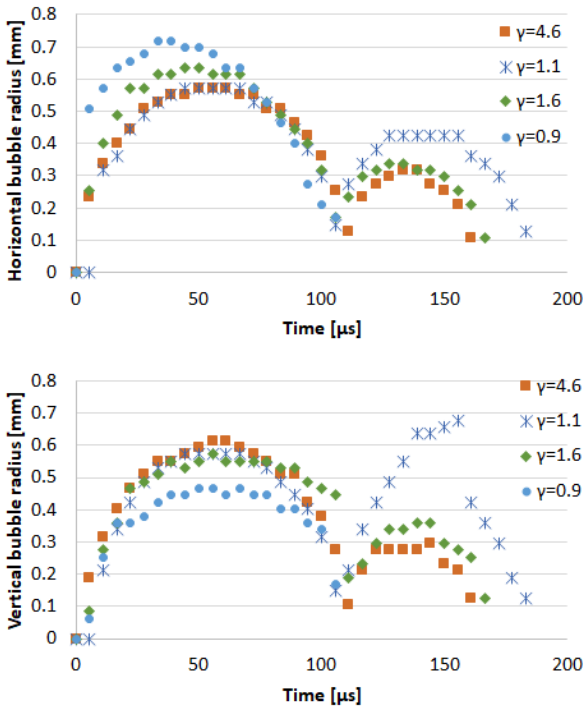

Fig. 7. Bubble radius in horizontal and vertical direction.

From the signal it is possible to identify several phenomena. In the first phase (up to 40 µs) the impact of the shock wave generated by the rapid plasma expansion is evident. The maximum bubble radius is reached about 70 µs. The bubble jet impact can be observed in the time

after the first bubble collapse. In the time frame from 100 µs to 120 µs the first bubble collapse can be identified. The second bubble collapse can be identified in time about 180 µs.

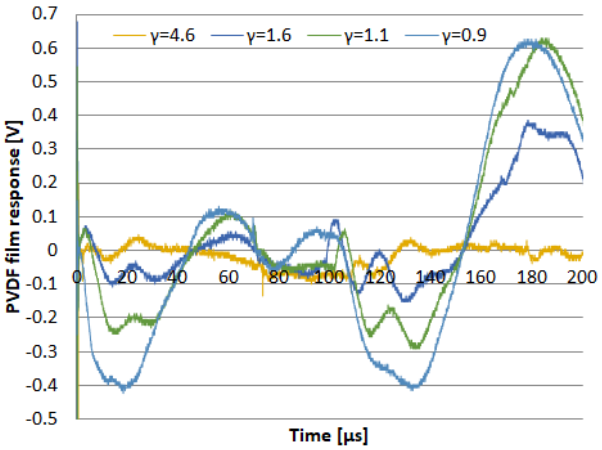

Fig. 8. Voltage signal measured on the PVDF film.

4 Conclusion

The cavitation bubble dynamic in the case of flexible wall exhibits completely different behaviour in the comparison to the rigid wall. The bubble jet generated during the bubble rebound can be generated for the flexible wall either towards the wall or from the wall. Also, the bubble is attracted either towards the wall or moves from the wall. The signal generated on the flexible wall indicated that the second bubble collapse is more intensive than the first bubble collapse.

Note that the cavitation bubble dynamic was investigated only for one set of elastic properties of the wall. It is known from the literature that the value of the wall elastic modulus can influence the bubble dynamic significantly. The investigation should be extended by the matrix of maximum bubble radii and the elastic moduli. The other part of the research should be focused to appropriate calibration method of the PVDF film sensor to obtain pressure of force value instead of the voltage signal.

The usage of the PVDF film sensor directly as the flexible wall represents a unique solution, which enables the possibility for the quantification of the bubble-flexible wall interaction without modification of the wall properties.

Acknowledgements

This research was supported by the Student Grant Competition of the Technical University of Liberec, grant number SGS-2019-5703 (21291) „ Experimental, numerical and theoretical research in fluid mechanics and thermomechanics“, grant number SGS-2020-5028 (21397) „Investigation of cavitation collapse by PVDF sensors“ and by the Ministry of Education, Youth and Sports of the Czech Republic, grant number 8J19FR018 „Assessment of the damage potential of cavitation for industrial hydraulic applications”. Authors would like to acknowledge the help of Darina Jašíková and Michal Kotek from the Institute for Nanomaterials, Advanced Technologies and Innovation.

References

1. P. K. Kennedy, D. X. Hammer, and B. A. Rockwell, Prog. Quantum Elec-tron. **21** (3), pp. 155–248 (1997)
2. T. Juhasz, X.N. Hu, L. Turi, and Z. Bor, Lasers in Surgery and Medicine **15** (1), pp. 91-98 (1994)
3. E. A. Brujan, *Proceedings of the Romanian Academy-Series A: Mathematics, Physics, Technical Sciences, Information Science* **6**, pp. 155-160 (2005)
4. E. A. Brujan, Medical Engineering and Physics **31** (7), pp. 742-751 (2009)
5. A. Vogel, R. Engelhardt, U. Behnle and U. Parlitz, Appl Phys B **62**, pp. 173–182 (1996)
6. D. X. Hammer, R. J. Thomas, M. Frenz, E. Jansen, G. D. Nojin, S. J. Giggs, J. Noack, A. Vogel and B. A. Rockwell, *Proc. SPIE 2681 "Laser Tissue Interaction VII"*, pp. 437-448 (1996)
7. J. P. Franc and J. M. Michel, *Fundamentals of cavitation*. Kluwer Academic Publishers, Boston, ISBN 14-020-2232-8 (2004)
8. C. E. Brennen, *Cavitation and bubble dynamics*, New York: Oxford University Press, 282 p., ISBN 978-0195094091 (1995).
9. A. Vogel, J. Noack, K. Nahen, D. Theisen, S. Busch, U. Parlitz, D. X. Hammer, G. D. Noojin, B. A. Rockwell and R. Birngruber, Appl Phys B **68**, pp. 271–280 (1999)
10. D. C. Gibson and J. R. Blake, *Australasian Conference on Hydraulics and Fluid Mechanics*, pp. 283-286 (1980).
11. D. C. Gibson and J. R. Blake, Appl. Sci. Res. **38**, pp. 215–224 (1982).
12. T. Kodama and Y. Tomita, Appl Phys B: Lasers Opt. **70**, pp. 139–149 (2000)
13. A. Shima, Y. Tomita, D.C. Gibson and J.R. Blake, J. Fluid Mech. **203**, pp. 199–214 (1989)
14. E. A. Brujan, K. Nahen, P. Schmidt and A. Vogel, J Fluid Mech **433**, pp. 251–281 (2001)
15. D. Obreschkow, M. Tinguely, N. Dorsaz, P. Kobel, A. de Bosset, M. Farhat, Experiments in Fluids **54** (4), pp. 1-18